A Mutation of β-Actin That Alters Depolymerization Dynamics Is Associated with Autosomal Dominant Developmental Malformations, Deafness, and Dystonia

Vincent Procaccio,[1,2,*] Gloria Salazar,[3,*] Shoichiro Ono,[4] Melanie L. Styers,[3] Marla Gearing,[4] Antonio Davila,[1] Richard Jimenez,[1] Jorge Juncos,[5] Claire-Anne Gutekunst,[6] Germana Meroni,[7] Bianca Fontanella,[7] Estelle Sontag,[8] Jean Marie Sontag,[8] Victor Faundez,[3] and Bruce H. Wainer[4]

[1]Center for Molecular and Mitochondrial Medicine and Genetics (MAMMAG), and [2]Department of Pediatrics, University of California, Irvine; Departments of [3]Cell Biology, [4]Pathology and Laboratory Medicine, [5]Neurology, and [6]Neurosurgery, Emory University School of Medicine, Atlanta; [7]Telethon Institute of Genetics and Medicine (TIGEM), Naples, Italy; and [8]Department of Pathology, University of Texas Southwestern Medical Center, Dallas

Actin, one of the major filamentous cytoskeletal molecules, is involved in a variety of cellular functions. Whereas an association between muscle actin mutations and skeletal and cardiac myopathies has been well documented, reports of human disease arising from mutations of nonmuscle actin genes have been rare. We have identified a missense point mutation in the gene coding for β-actin that results in an arginine-to-tryptophan substitution at position 183. The disease phenotype includes developmental midline malformations, sensory hearing loss, and a delayed-onset generalized dystonia syndrome in monozygotic twins. Cellular studies of a lymphoblastoid cell line obtained from an affected patient demonstrated morphological abnormalities of the actin cytoskeleton and altered actin depolymerization dynamics in response to latrunculin A, an actin monomer–sequestering drug. Resistance to latrunculin A was also observed in NIH 3T3 cells expressing the mutant actin. These findings suggest that mutations in nonmuscle actins may be associated with a broad spectrum of developmental malformations and/or neurological abnormalities such as dystonia.

Actin, one of the major cytoskeletal proteins, participates in many important cellular functions, including muscle contraction, cell motility, cytokinesis, vesicle and organelle movement, cell signaling, and the establishment and maintenance of cell junctions and cell shape.[1–5] It is highly conserved throughout evolution because it interacts with a large number of proteins.[1] The actin family comprises three major isoform groups based on electrophoretic mobility: α-actin, β-actin, and γ-actin.[6] In mammalian cells, there are six isoforms coded by separate genes, consisting of four muscle isoforms (α-skeletal, aortic smooth, cardiac, and γ2-enteric) and two nonmuscle actins (β and γ1).[7] Whereas cellular actin may be altered in various disease states and in aging,[8–10] >60 mutations of the skeletal (*ACTA1*) and cardiac (*ACTC*) muscle actin genes have been identified in hereditary muscle diseases.[11–13] The majority of *ACTA1* mutations are dominant, a small number are recessive, and most isolated cases in individuals with no previous family history are de novo dominant mutations.[11] In contrast, reports of nonmuscle actin mutations have been limited to two reports of the γ-actin gene (*ACTG1*) in familial deafness[14,15] and the β-actin gene (*ACTB*) in a single patient with recurrent infections.[16] However, no neurodegenerative syndromes or ventral midline–defect phenotypes have been linked to mutations in vertebrate nonmuscle actin genes.

Dystonia is a movement disorder syndrome characterized by sustained involuntary muscle contractions that cause abnormal postures and repetitive movements.[17,18] To date, genetic loci have been identified in at least 12 autosomal dominant forms, and the specific disease genes have been identified in 5 autosomal dominant forms, in 1 X-linked form, and in 1 autosomal recessive form.[19] Here, we report that a mutation in the nonmuscle isoform *ACTB* is associated with a combination of ventral midline malformations, sensory hearing loss, and delayed-onset generalized dystonia.

Material and Methods

Patient Tissues and Cell Lines

The neuropathology of the probands was reported elsewhere.[20] At the time of the brain autopsy, tissue samples were frozen immediately on metal plates previously cooled in a −80°C freezer. The frozen samples were then stored at −80°C.

Received November 11, 2005; accepted for publication March 9, 2006; electronically published April 21, 2006.

Address for correspondence and reprints: Dr. Vincent Procaccio, Center for Molecular and Mitochondrial Medicine and Genetics, Hewitt Hall, Room 2034, University of California, Irvine, Irvine, CA 92697-3940. E-mail: vproca@uci.edu

* These two authors contributed equally to this work.

Am. J. Hum. Genet. 2006;78:947–960. 0002-9297/2006/7806-0006$15.00

The remainder of the brain tissue was fixed in neutral buffered formalin at room temperature, sections were taken for paraffin embedding, and the remaining formalin-fixed tissue was stored in sealed plastic bags at room temperature. Between the deaths of the first and second probands, blood samples were obtained with informed consent from the surviving proband, the mother, and the two half-brothers. Buffy coat fractions were obtained and transformed using Epstein-Barr virus, in accordance with standard published procedures.[21] Lymphoblastoid cell lines from the patient, first-degree relatives, and controls were passaged in RPMI 1640 supplemented with additional glucose (final concentration 4.5 mg/ml), 10% fetal bovine serum, 50 μg/ml uridine, and 1 mM pyruvate.

DNA Sequencing and Mutation Analysis

DNA was extracted from brain tissues, cell lines, and blood samples with the use of a Puregene kit (Gentra Systems). Total RNA was extracted from brain tissue and lymphoblast cell lines with the use of TRIzol, was treated with DNAse I, was purified using a RNAeasy kit (Qiagen), and was reverse transcribed using a first-strand cDNA kit (Invitrogen).

The *ACTB* gene (GenBank accession number M10277), *ACTB* cDNA (GenBank accession number NM_001101), *ACTG1* cDNA (GenBank accession number NM_001614), cofilin 1 (*CFL1*) cDNA (GenBank accession number NM_005507), and actin depolymerizing factor (*ADF*) cDNA (GenBank accession number NM_006870) were amplified using standard conditions and were sequenced with primers chosen from the cDNA or genomic DNA reference sequences (table 1). PCR products were treated with ExoSAP-IT (Amersham), to remove primers and unincorporated nucleotides before sequencing. Sequencing reactions were performed with the ABI PRISM Big Dye Terminator Cycle Sequencing v3.0 Ready Reaction Kit and were analyzed on an ABI 3100 DNA Analyzer (Applied Biosystems). To identify single polymorphisms occurring in normal controls, we sequenced exon 4 of *ACTB* in 117 DNA samples derived from unrelated control individuals, of the same ethnicity as the patient, who had no neurological or malformation disorders.

The patients were previously screened for torsion dystonia-1 (*DYT1*) gene mutations as well as for the dystonia/deafness-1 (*DDP1*) mutation, and the results were negative.[20] Results from mitochondrial respiration studies performed after muscle biopsies were negative as well. The patients also exhibited clinical features found in Opitz syndrome (OS [MIM 300000]), including ventral midline abnormalities such as esophageal motility problems and hypertelorism. We therefore screened for genetic abnormalities known to be associated with this syndrome.[22] The nine coding exons of the *MID1* gene were amplified using primers and conditions described elsewhere to evaluate the X-linked form of the syndrome.[23,24] To evaluate the chromosome 22–linked form of the syndrome,[25] FISH analysis was performed on metaphase lymphoblastoid cells from the patient, with the use of the N25 and *TUPLE1* probes (Appligene Oncor) in accordance with the manufacturer's instructions.

Table 1

Primer Sequences for the *ACTB* Gene and for *ACTB, ACTG1, CFL1,* and *ADF* cDNAs

The table is available in its entirety in the online edition of *The American Journal of Human Genetics*.

Electrophoresis/Immunoblotting

Brain tissues stored at −80°C were pulverized in the presence of liquid nitrogen before homogenization. Lymphoblasts were harvested and were washed twice with PBS, and the cell pellets were stored frozen at −80°C. They were lysed in 3–4 vol of SDS sample buffer (2% SDS, 80 mM Tris, 5% β-mercaptoethanol, 15% glycerol, and 0.05% bromophenol blue [pH 6.8]), were heated at 97°C for 2 min, were homogenized by brief sonication, and were heated again at 97°C for 2 min. Protein concentrations of the lysates were determined by a filter paper dye-binding assay.[26] For one-dimensional SDS-PAGE, the lysates were used directly for analysis. Samples were loaded into the gel lanes in equal protein concentrations, with an additional lane employed as a "loading control" (probed for tubulin). For two-dimensional electrophoresis, proteins in the lysates were precipitated by the method described elsewhere[27] to remove SDS, were resuspended in isoelectric focusing (IEF) sample buffer (8 M urea, 2% CHAPS, 50 mM dithiothreitol, and 0.2% Bio-Lite 3/10 ampholytes) with brief sonication, and were applied to pH 4–7 ReadyStrip immobilized pH gradient (IPG) strips (11-cm gel [Bio-Rad]) by passive rehydration. IEF was performed by applying 35,000 V/h, with a maximum voltage of 8,000 V, with the use of Protean IEF cell (Bio-Rad). The IPG strips were equilibrated in equilibration buffer I (6 M urea, 0.375 M Tris-HCl [pH 8.8], 2% SDS, 20% glycerol, and 2% dithiothreitol) for 10 min and then in equilibration buffer II (6 M urea, 0.375 M Tris-HCl [pH 8.8], 2% SDS, 20% glycerol, and 2.5% iodoacetamide) for 10 min and were applied to SDS-PAGE (12% acrylamide gel) for the second dimension. The proteins from SDS-PAGE were transferred to Immobilon-P (0.2 μm) membranes. After incubation in blocking solution (Tris-buffered saline [pH 7.4], 0.025% Triton X-100, and 5% powdered milk), membranes were rinsed and incubated overnight at 4°C with either anti–β-actin (mouse monoclonal clone AC-15 [Sigma]), anti–γ-actin (sheep [Chemicon]), anti–pan-actin (mouse monoclonal clone AC-40 [Sigma]), or anti–α-tubulin (monoclonal mouse clone DMIA [Sigma]). All antibodies were used in the 1:1,000–1:2,000 dilution range. After several rinses, the membranes were incubated for 1 h at room temperature with appropriate horseradish peroxidase (HRP)–labeled secondary antibodies: HRP goat anti-sheep (1:5,000 [Zymed]) and HRP donkey anti-sheep IgG (1:7,000 [Jackson Immunoresearch Labs]). The membranes were then rinsed, and proteins were visualized using chemiluminescence (ECL [Amersham Biosciences]). The x-ray film was exposed to the membranes for varying time intervals ranging from 5 s to 10 min. The developed films were scanned for image archiving and for densitometry measurements.

Coverslip Cultures/Phalloidin Staining and Immunofluorescence

Lymphoblast cell lines (sex- and age-matched control and patient) were grown in RPMI 1640 supplemented with uridine (5 μg/100 ml), gentamycin sulfate (0.05 mg/ml), and 20% fetal bovine serum (Hyclone) in 25-cm^2 flasks under a 5% CO_2 humidified incubator at 37°C. Cells were seeded on coverslips previously coated with the combination of 0.01% poly-L-lysine (Sigma) and 20 μg/well of fibronectin (Invitrogen) in growth medium. After 24 h in culture, cells were incubated for 24 h in medium containing 1% bovine growth serum. They were then treated for 3 h with or without 0.25 μg/ml latrunculin A (Molecular Probes). Cells were then fixed for 20 min in 4% paraformaldehyde (PFA) in PBS, were permeabilized for 5 min in 0.1% Triton X-100 in PBS, and were processed for visualization of filamentous actin with the use of Alexa Fluor 488 conjugated phalloidin (1:100 [Molecular Probes]),[28] or tetramethylrhodamine-phalloidin (Sigma) at 0.1 μg/ml. The samples were mounted with Fluoromount (Fisher) and were examined on a Zeiss microscope equipped with a 100× objective. Images were directly captured and were transferred to Adobe Photoshop CS for printing.

For immunofluorescence, coverslip cultures were fixed either with PFA, as described above, or with ice-cold methanol for 10 min. After rinsing and permeabilization, cells were incubated with antibodies to either β-actin (AC-15, 1:1,000 dilution [Sigma]) or γ-actin (sheep, 1:7,000 dilution [Chemicon]) for 1 h at room temperature. Coverslips were then rinsed and were stained with appropriate secondary antibodies (Alexa Fluor 488 goat anti-mouse IgG, 1:5,000 dilution; Alexa Fluor 568 donkey anti-sheep IgG, 1:5,000 dilution [Molecular Probes]) for 1 h at room temperature. The coverslips were then rinsed and mounted. The slides were examined in a Leica DMR microscope, and images were captured with a digital camera and a Zeiss LSM50 confocal microscope. Images were processed using Adobe Photoshop and Zeiss LSM software.

Flow Cytometry

Lymphoblast cell lines (control and patient) were treated with and without latrunculin A for 15 min at 37°C, were rinsed in PBS, and were fixed in 4% PFA for 20 min. After permeabilization in 0.025% Triton X-100 in PBS, cells were incubated with Alexa Fluor 488 phalloidin for 30 min at 37°C and were resuspended in PBS. Actin filaments stained with phalloidin were analyzed using an analytical flow-cytometry system (BD Biosciences). The results were analyzed using Flojo version 6.0 (Treestar).

Latrunculin A Studies on Transfected 3T3 cells

To verify that the R183W mutation in the patient lymphoblasts was responsible for the resistance to latrunculin A, we performed similar studies using NIH 3T3 cells stably transfected with green fluorescent protein (GFP)–tagged constructs of mutant and wild-type β-actin. A cDNA construct encoding full-length human β-actin was generated by RT-PCR and was introduced into a plasmid pEGFP vector (BD Biosciences). Expression of the R183W substitution in the β-actin construct was introduced by site-directed mutagenesis, with use of the QuikChange XL Site-Directed Mutagenesis Kit (Stratagene) with a pEGFP vector as a template plasmid harboring the entire coding sequence of β-actin. Clones were confirmed to contain the desired mutation by DNA sequence analysis. NIH 3T3 cells were transfected with the wild-type and mutant constructs with the use of standard commercial reagents (Effectene [Qiagen]) and were grown in selection media containing the neomycin analogue, G418. The transfected cells that survived selection demonstrated ~30% positivity for GFP fluorescence when examined under epifluorescence. Populations of cells enriched (>80%) for efficient transgene expression were obtained using preparative fluorescence-activated cell sorting at the Yerkes Primate Facility at Emory. The sensitivity of transfected cells to the depolymerizing actions of latrunculin A was initially evaluated on live cell preparations with the use of confocal microscopy. Briefly, the cells were plated at low density onto chambers containing glass-bottomed wells that had been previously coated with growth-factor–free commercial substratum (Matrigel) and were allowed to attach for 3 h. After attachment, the medium was replaced with low-serum medium (1%), and cells were allowed to incubate overnight. Chambers were then rinsed, the medium was replaced with phenol-free medium plus Hepes buffer, and they were placed on the stage of an inverted Zeiss LSM 510 confocal microscope system, which was fitted with an objective warming collar and used immersion oil designed for the warming environment. Microscopic fields containing GFP fluorescence associated with the actin stress-fiber networks were selected using a 40× oil objective, and several pre-drug images were captured. Latrunculin A was then added to the chambers for final concentrations of either 250 or 500 ng/ml, and the fields were scanned at intervals of 1 min, for up to 30 min. Image series were then evaluated using LSM software. Control chambers in which no drug was added demonstrated that the stress fiber–associated fluorescence remained stable over the 30-min incubation period. On the basis of an examination of the real-time images, quantitative experiments were performed on duplicate coverslip cultures of the transfected cells with the use of a final latrunculin A concentration of 250 ng/ml. Coverslips were rinsed and were fixed with ice-cold methanol at intervals of 5, 10, 15, and 20 min after drug addition. Coverslip cultures without drug treatment were included as controls. All processed coverslips were mounted onto glass microscope slides with the use of gelvatol and were examined using the Zeiss LSM 510 confocal microscope. For each coverslip, five random fields of cells were scanned using a 40× oil objective, and the images were analyzed using Metamorph software to compute the fluorescence intensity of individual cell profiles as a percentage of cell area. The collected data was analyzed statistically with the use of the Student *t* test.

Results

Genetic Studies

The probands whom we reported elsewhere were born with several ventral midline malformations, including cleft palate and lip, hypertelorism, and esophageal motility problems.[20] The hearing loss was first reported in

primary school, was documented by audiometric testing, and was confirmed through periodic follow-up by otolaryngological specialists. The hearing loss was severe and bilateral, eventually necessitating the use of sign language to communicate. Beginning in early adolescence, the patients developed a progressive generalized dystonia syndrome that led to death in their early twenties due to repeated episodes of aspiration pneumonia. As reported elsewhere, genetic testing results for *DYT1* mutations associated with one of the forms of primary dystonia[18] were negative, as were results for the *DDP1* mutation and known mitochondrial disorders.[20] The constellation of malformations exhibited by the patients resembles OS.[22] We searched for mutations in *MID1,* the gene responsible for the X-linked form of OS (XLOS),[23] and found no mutations in the nine coding and splice-site regions of this gene (data not shown). OS is genetically heterogeneous, and an autosomal dominant form (ADOS) has also been identified. Although the gene implicated has not been discovered yet, ADOS has been mapped to chromosome 22.[22] Patients with ADOS usually show a large chromosomal deletion in the long arm of chromosome 22—in particular, in the DiGeorge region (22q11.2).[25] For this reason, we performed FISH analysis with the use of two different probes for the 22q11.2 region on lymphoblastoid cells of the proband. Both probes revealed that no large deletions are present in the patient cells (fig. 1).

Postmortem brain examinations of both patients revealed a remarkable pathology consisting of abundant proteinaceous inclusions that stained positively for actin and for the actin regulatory protein, cofilin.[20] Therefore, genes coding for actin and actin regulatory proteins, such as *ADF* and *CFL1,* were sequenced using cDNAs obtained from reverse-transcribed mRNA from the brains of both twins and from the lymphoblast cell line of the second twin (table 1). A heterozygous missense point mutation was identified in *ACTB,* which was confirmed by sequencing genomic DNA. As illustrated in fig. 2*A*, a sequence electrophoregram of the genomic sequence from exon 4 identified a heterozygous base change of cytosine to thymine at nucleotide position 547C→T. This change predicts an amino acid substitution of arginine (R) to tryptophan (W) at position 183 in the β-actin molecule (R183W), which is highly conserved across species (fig. 2*B*). No mutations were identified in the remaining five *ACTB* exons, in *ACTG1,* or in *ADF* and *CFL1* cDNAs (table 1). Similarly, no mutations in *ACTB* or other related genes were identified in the mother and the two half brothers. Paternal samples were not available for analysis, but there is no paternal family history of similar disorders. The patients had the appearance of identical twins, and we have confirmed monozygosity with DNA microsatellite analysis, by typing a series of polymorphic loci (fig. 3*A*). In addition, a series of microsatellite markers in close proximity to *ACTB* on chromosome 7 was used to trace the inheritance of *ACTB* alleles over generations. Individuals were genotyped for markers on chromosome 7 bracketing the disease locus. Segregation analysis of microsatellite markers flanking *ACTB* demonstrates the inheritance of maternal chromosomes in the affected twins and an unaffected half brother (fig. 3*B*).

The figure is available in its entirety in the online edition of *The American Journal of Human Genetics.*

Figure 1 FISH analysis of metaphase lymphoblast cells from the proband, with DiGeorge markers for chromosome 22. The legend is available in its entirety in the online version of *The American Journal of Human Genetics.*

Mutations in skeletal muscle α-actin at this same position, R183, with different amino acid substitutions, cysteine or glycine, are associated with severe myopathies.[11] In addition, a double mutant—R183A-D184A, which does not confer an obvious cytopathic phenotype in yeast[29]—was shown to induce resistance to the actin depolymerizing agent, latrunculin A, both in yeast[30] and in mammalian cells.[31] The 547C→T substitution was not detected in sequence analysis of exon 4 of *ACTB* in 117 DNA control samples from a population of the same ethnicity. Similarly, the R183W substitution was not found in searches of databases reporting known polymorphisms in *ACTB* (dbSNP). These results argue against the possibility that the R183W substitution represents a genetic polymorphism.

Biochemical Studies

The R183W substitution predicts a gene product with a more acidic isoelectric point than its wild-type counterpart. To test this hypothesis, we investigated the expression of mutant versus wild-type protein in brain and lymphoblast cell lysate samples, using two-dimensional gel electrophoresis and immunoblot analysis. As illustrated in figure 4*A*, wild-type β- and γ-actin migrate according to predicted isoelectric points (pI) of 5.29 and 5.31, respectively (Expasy Proteomics Server), and a molecular size of 42 kDa. In cortical brain specimens from both patients, a second, more acidic β-actin species with a predicted pI of 5.21 was present at approximately equal levels with wild-type. These findings are consistent with the predicted R183W substitution. In contrast, probing for γ-actin revealed only the wild-type species. Similarly, wild-type and mutant β-actin were detected in the immunoblots from two-dimensional gels of lymphoblastoid cell lysates from the second patient (fig. 4*B*) but not in those from a control sample or the mother. It has been demonstrated elsewhere that the expression levels

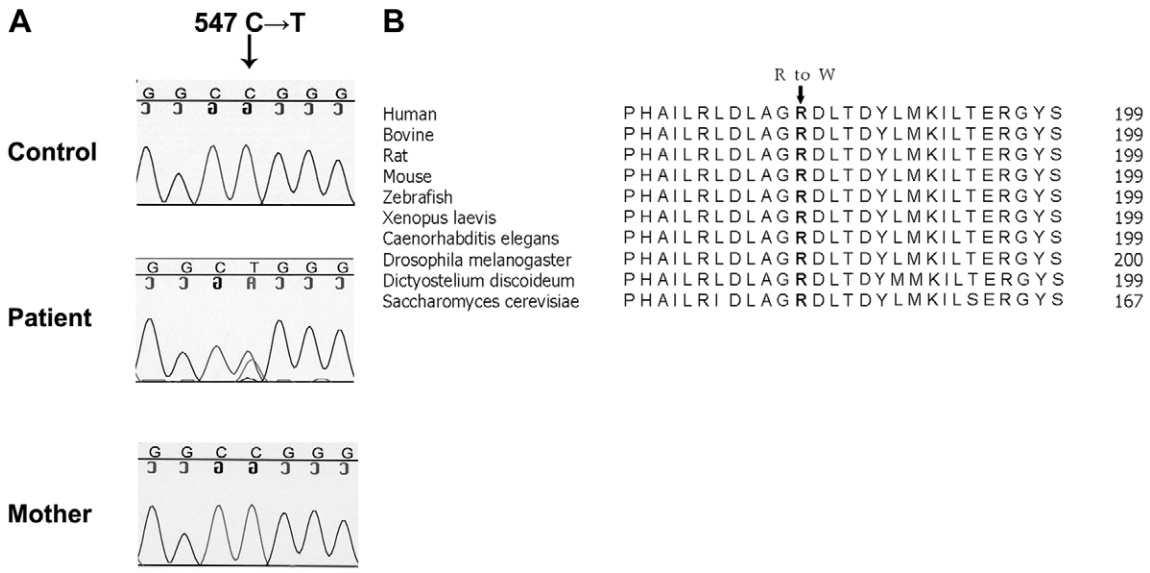

Figure 2 Identification of the mutation in the gene coding for β-actin. *A,* Partial sequence of exon 4 of *ACTB* in a control, the patient, and the patient's mother. The sequences illustrated in the control and mother are no different than the sequence found in 117 ethnicity-matched control samples of this region of the gene and in the two half-brothers. The patient shows a heterozygous CGG-to-TGG transition, which predicts an R183W substitution. *B,* Sequence conservation of the β-actin sequence among different species. Alignment of amino acid sequences in the region of the identified R183W substitution indicates the strict conservation of an arginine residue at position 183 in all species assessed, from yeast to man.

of actin pools are autoregulated, even in the presence of mutant actin species.[32,33] We therefore examined whether our newly identified mutation would behave similarly. Brain samples and cell lysates were subjected to SDS-PAGE and immunoblot analysis probing for β-, γ-, and total actin, with the use of an antibody recognizing all isoform species. We observed no apparent difference in the expression levels of these markers in patient versus control samples (fig. 4*C* and 4*D*). Densitometric measurements of band intensity did not show any differences (data not shown). These findings suggest that the R183W substitution does not alter β-actin stability or induce compensatory changes in the expression of other actin isoforms.

Morphological Studies

The morphology of the lymphoblastoid cell lines was examined using both brightfield microscopy, phalloidin staining, and immunofluorescence of actin isoforms. Control cells exhibited a rounded morphology and lamellapodia with microspikes, as well as some small filopodia (fig. 5*A*), and the pattern of filamentous actin was most concentrated in the cell cortex (fig. 5*B*). In contrast, cells expressing the mutant β-actin exhibited variations in cell shape, with long tapering processes extending for distances greater than a cell diameter (fig. 5*C* and 5*D*). Immunofluorescence for β- and γ-actin and merged images (fig. 5*E*–5*G* for control cells and fig. 5*H*–5*J* for patient cells) revealed the same differences in cell morphology in the patient cells. In both wild-type and mutant cells, the actin visualization was most intense at the cell cortex, and the relative fluorescence intensities were similar for β- and γ-actin, exhibiting a strong colocalization pattern.

Molecular Modeling and Interactions with Phalloidin versus Latrunculin A

The structural effect of the R183W substitution was examined by modeling the mutation in known actin structures. Furthermore, we used previous mutational analyses on the binding of actin-disrupting drugs, to test predictions of the R183W model. A molecular model of the β-actin monomer region containing residue 183, based on the crystal structure from *C. elegans*[34] (fig. 6*A*), illustrates the arginine residue (183) positioned directly across from the ATP-binding pocket. This residue can

The figure is available in its entirety in the online edition of *The American Journal of Human Genetics.*

Figure 3 Microsatellite analysis of proband family pedigree, to determine monozygosity of probands with the use of random chromosome microsatellite markers and markers for chromosome 7. The legend is available in its entirety in the online version of *The American Journal of Human Genetics.*

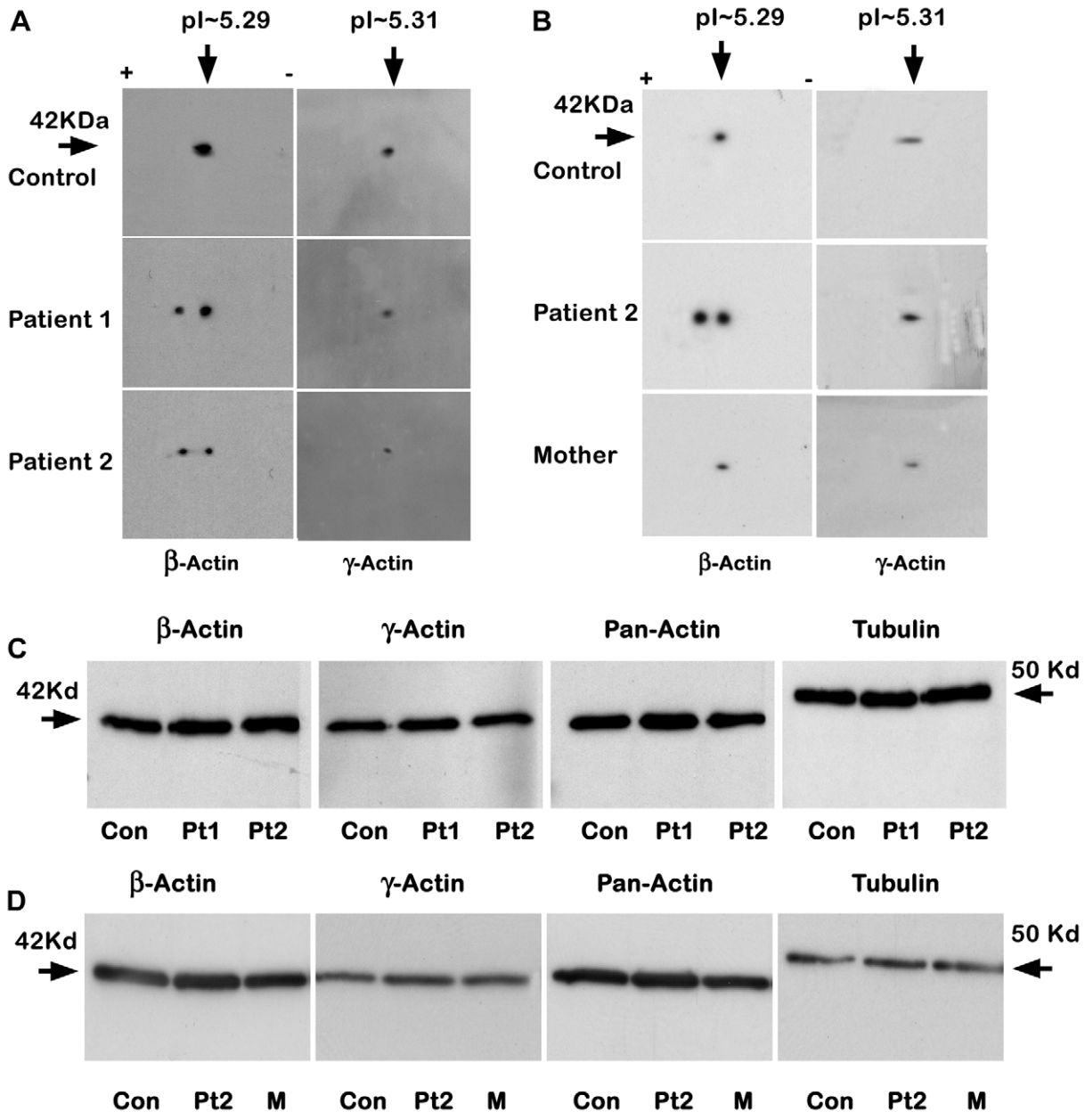

Figure 4 Two-dimensional and SDS-PAGE gel-immunoblot analyses of β- and γ-actins in brain samples and cell lysates. *A*, Immunoblots from two-dimensional gels probed for β- and γ-actin in brain samples from an age-matched control and both patients. *B*, Immunoblots from two-dimensional gels probed for β- and γ-actin in lymphoblast cell lysates from an age-matched control, patient 2, and the patient's mother. *C* and *D*, Brain samples from both patients and cell lysate from the second patient, in which two species of β-actin are present in equal amounts, consistent with heterozygosity. The theoretical pIs for wild-type and mutant β-actin (R183W) are 5.29 and 5.21 (Expasy). Only wild-type γ-actin with a theoretical pI of 5.31 was detected in brain and cell lysates from all individuals. Immunoblots are shown from SDS-PAGE analysis of brain samples (*C*) and cell lysates (*D*) from controls, patients, and mother. The relative levels of β- versus γ- and total actin did not show any differences between controls, mother, and patients in the samples tested. All gel lanes were loaded with equal protein concentrations, and α-tubulin was probed as a protein loading control.

potentially participate in a hydrogen-bonded network with water molecules and *Ser*14/*His*73, which can form a flexible gatelike structure facilitating ATP exchange within the cleft.[35] The R183W substitution (fig. 6*B*) could theoretically disrupt the hydrogen bonds by introducing the hydrophobic tryptophan side chain. Such a change could potentially alter the ATP-binding pocket without affecting the overall structure (fig. 7). We pre-

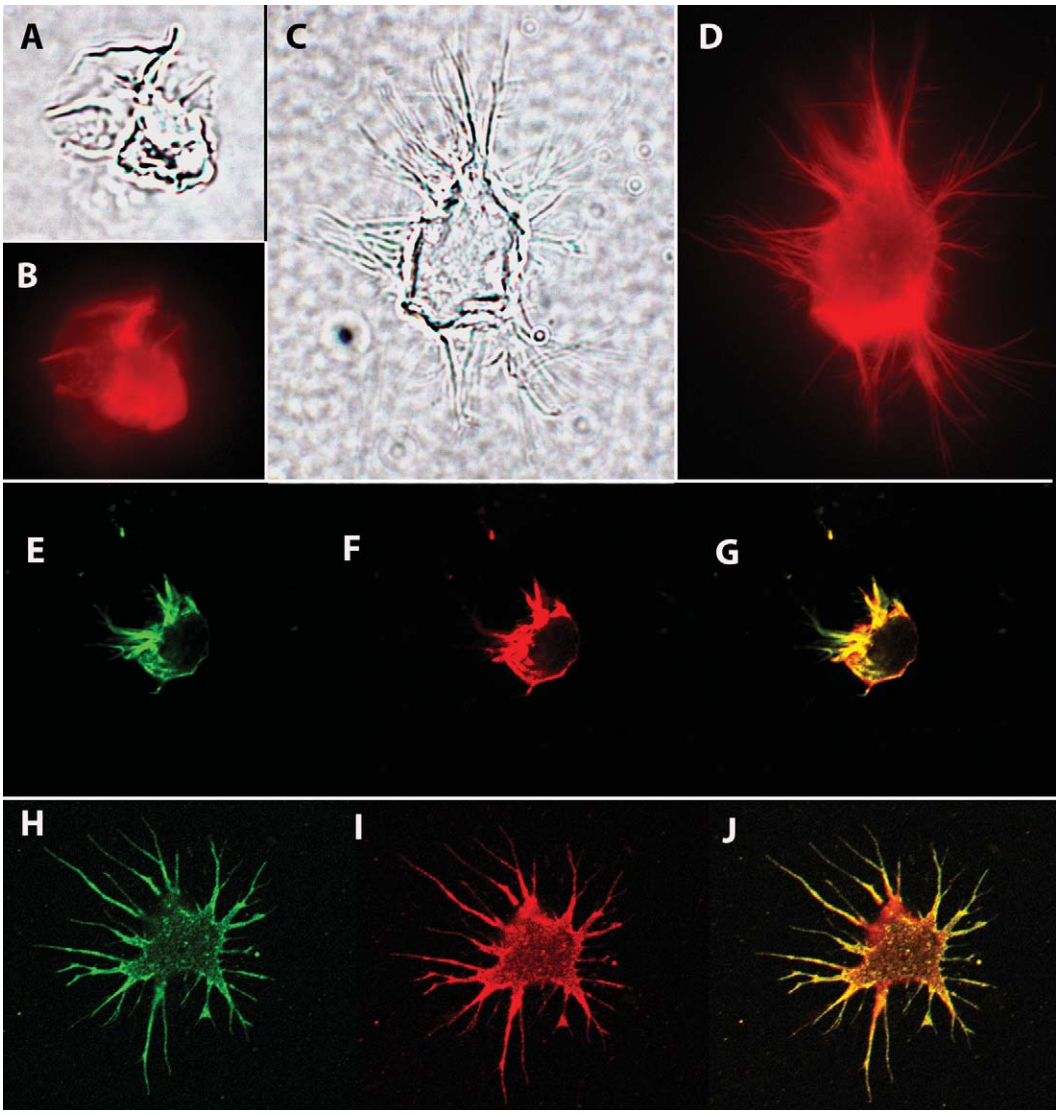

Figure 5 Brightfield microscopy, phalloidin staining, and immunofluorescence for β- and γ-actins in patient and control lymphoblastoid cell lines. Brightfield phase-contrast images of control (*A*) and patient (*C*) lymphoblasts illustrate the rounded morphology with lamellapodia and microspikes observed in control cells, in contrast to the extensive process formation observed in many of the patient cells. Epifluorescence images of Alexa Fluor 488 phalloidin staining in the same cells from control and patient illustrate actin-rich microspikes in the control cells (*B*) and actin filaments in long filopodial processes in the patient cells (*D*). Immunofluorescence confocal images of control cells stained for β-actin (*E, green*) and γ-actin (*F, red*). Both actin species are enriched in cortical regions and within microspikes and short filopodia (*G, merged images*). Immunofluorescence confocal images of a patient cell stained for β-actin (*H, green*) and γ-actin (*I, red*). Both actin species are enriched in cortical regions and within long filopodial processes (*J, merged images*). All cells were viewed with a 100 × oil objective.

dicted from the model that the binding of drugs whose recognition sites lie away from this region should remain unaffected. Phalloidin binds to a site on subdomain III and stabilizes actin filaments. The phalloidin-binding domain is removed from the ATP pocket (fig. 7). To test our prediction, we performed quantitative flow-cytometry analysis to determine the binding of Alexa-labeled phalloidin to fixed control and patient lymphoblasts and found no differences (fig. 6*C* and 6*D*).

In contrast to normal phalloidin binding, the R183W substitution modified the response of cells to actin monomer–sequestering drug latrunculin A, which binds close to the ATP-pocket[36,37] (fig. 7). Microscopic analysis of lymphoblasts treated with latrunculin A revealed that drug conditions leading to the depolymerization of the actin cytoskeleton in control lymphoblasts were less effective in cells carrying the R183W substitution (fig. 8). To assess this apparent resistance quantitatively, we

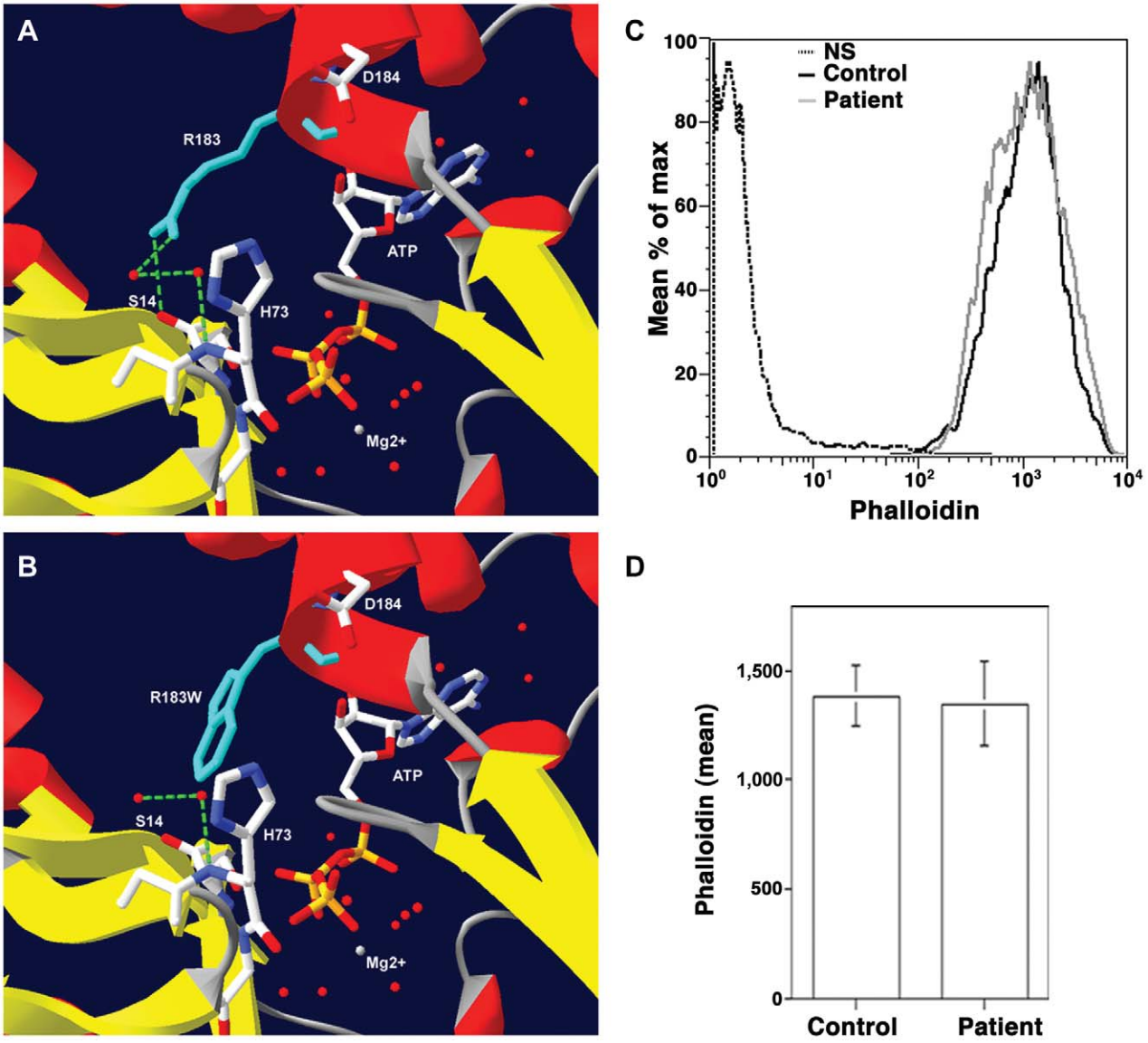

Figure 6 Molecular models of wild-type versus mutant actin and of phalloidin binding. *A,* Structure of globular actin monomer based on the crystal structure of actin from *C. elegans* (ACT1/3),[34] viewed using Deepview/Swiss PDB viewer (PDB accession number 1D4X). The ATP pocket region is magnified, and arginine 183 (*light blue*) lies directly across from the ATP-binding pocket. (see fig. 7 for an illustration of the entire monomer). *B,* R183W substitution disrupting the hydrogen-bonding network across the ATP-binding pocket of *C. elegans* actin. In addition, the tryptophan residue leads to a significant loss in flexibility of the residue. The most favorable rotamer predicted by the software is shown. *C,* Representative results of flow-cytometry measurements of phalloidin binding. Lymphoblast cell lines (control and patient) were fixed in PFA, were stained with phalloidin for 30 min at 37°C, and were analyzed by flow cytometry. No differences in actin filaments stained with phalloidin were observed between control and patient cells. NS = Fluorescence-background control samples where phalloidin was omitted. *D,* Analysis of the mean ± SD phalloidin binding for control (1,385 ± 138) and patient (1,349 ± 191) cell lines. $P_t = .8$ and $n = 10$ in three independent experiments.

treated the cells in suspension and measured the loss of phalloidin-stained filamentous actin, using flow cytometry. Consistent with the microscopy results, the mutant lymphoblasts were resistant to latrunculin A over a wide range of drug concentrations (fig. 9*A* and 9*B*). In contrast, when the drug was washed out, actin repolymerized to the same baseline levels in both control and mutant cells, irrespective of the extent of the la-

The figure is available in its entirety in the online edition of *The American Journal of Human Genetics*.

Figure 7 Structure of globular actin monomer. The legend is available in its entirety in the online version of *The American Journal of Human Genetics*.

trunculin-induced actin depolymerization (fig. 9*C* and 9*D*).

Resistance to Latrunculin A in Transfected 3T3 cells

Although the results of latrunculin A experiments performed using patient lymphoblastoid cells suggest that the R183W mutation was responsible for the resistance observed, it is also possible that nonspecific effects of the immortalization procedure may also have been responsible for the phenotype observed. In addition, it is possible that the affected twins harbor additional genetic abnormalities contributing to the phenotype, which has been documented in some cases of myoclonus-dystonia.[38] To test whether latrunculin A resistance in our patient lymphoblasts is a direct effect of the mutant β-actin expression, we prepared GFP-tagged constructs of wild-type and R183W β-actin and expressed them in NIH 3T3 cells. Latrunculin A sensitivity was then evaluated qualitatively on living cell cultures and quantitatively on methanol-fixed coverslip cultures. As illustrated in figure 10*A*, cells transfected with either the wild-type or R183W construct did not show any distinct differences in the morphology of their respective β-actin stress-fiber networks. However, after incubation in the presence of 250 ng/ml concentrations of latrunculin A, cells transfected with the wild-type constructs demonstrated stress-fiber loss by 15 min, whereas R183W-transfected cells were less altered. By 30 min, substantial stress-fiber loss was observed in the R183W-transfected cells, but the response was still less striking than that in cells transfected with the constructs (data not shown). At a higher latrunculin A dose, 500 ng/ml, cells expressing the mutant construct exhibited a faster loss of stress fibers but could still be distinguished from the wild-type cells (data not shown).

Latrunculin A resistance was examined quantitatively using coverslip cultures from either wild-type– or R183W-transfected 3T3 cells, which were treated for varying times with 250 ng/ml latrunculin A. As shown in figure 10*B*, cells transfected with the mutant construct exhibited resistance to the depolymerizing actions of the drug

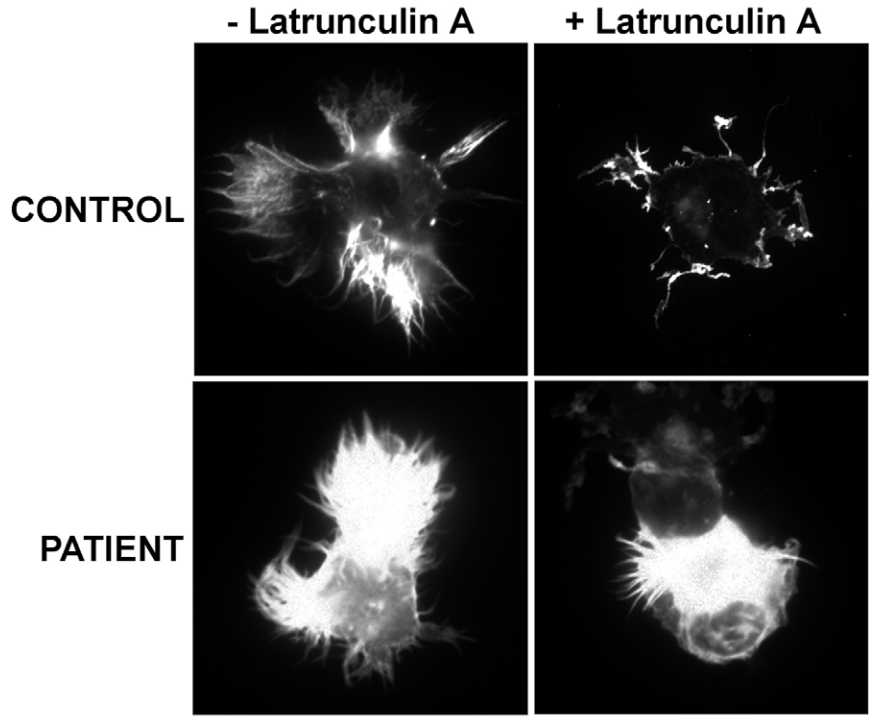

Figure 8 Effects of latrunculin A on attached mutant and control lymphoblasts. Control and patient lymphoblastoid cells were grown on coverslips in serum-deprived media and were treated with 250 ng/ml latrunculin A for 3 h. Treatment of control cells resulted in complete loss of filamentous actin visualized with Alexa Fluor 488 phalloidin staining. In contrast, filamentous actin is still present on patient cells after drug treatment.

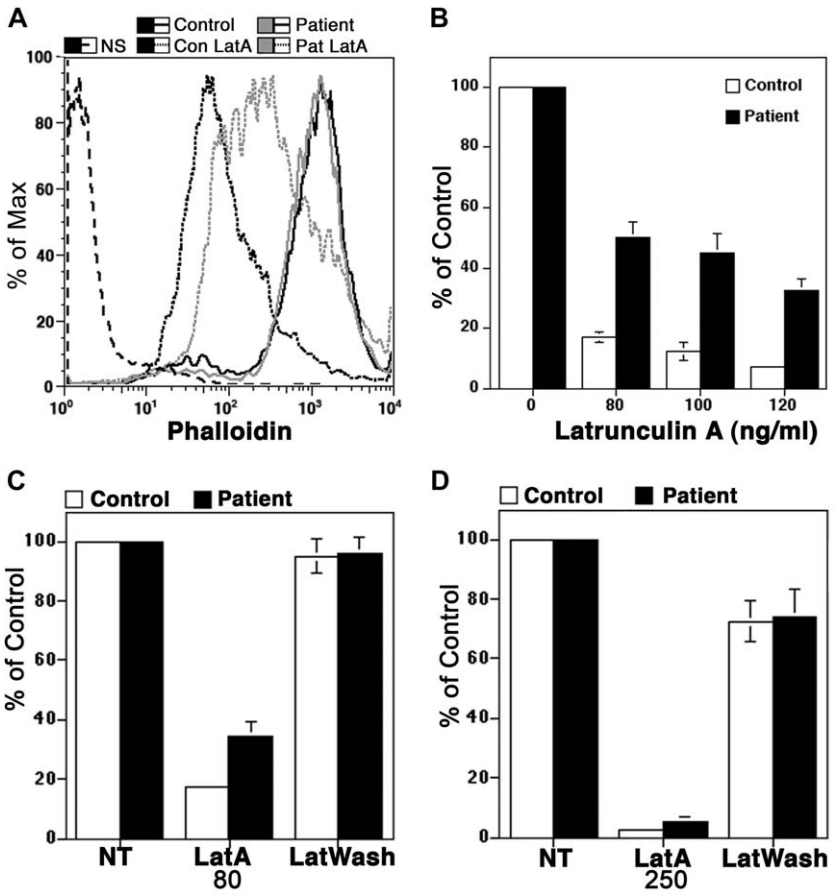

Figure 9 Quantitation of latrunculin A resistance in patient cells using flow cytometry. *A* and *B*, Both control and patient cells show similar actin filament content in nontreated cells. Latrunculin A treatment (80 ng/ml) induces a rapid actin depolymerization in control compared with patient cells. Actin filament content was reduced to 17% ± 1.8% and 50% ± 4.9% (average ± SD, $n = 8$) in control and patient, respectively. NS = Fluorescence-background control samples where phalloidin was omitted. *B*, Resistance of actin filaments in patient cells to depolymerization also observed by using increasing concentrations of latrunculin A. *C* and *D*, Recovery from latrunculin A. Cells were treated with 80 ng/ml of latrunculin A for 15 min, were washed, and were incubated with RPMI plus 10% fetal bovine serum for 5 min at 37°C (*C*). Cells were treated with 250 ng/ml latrunculin A for 30 min, were washed, and were incubated with RPMI plus 5% fetal bovine serum (*D*). Under both conditions, actin filament content recovered to 100% in both control and patient cells.

at 10 min ($P_t = .02$), at 15 min ($P_t < .0001$), and at 20 min ($P_t = .04$). These results demonstrate that the mutant actin species is responsible for the cellular phenotype.

Discussion

The results of the present studies indicate that a mutation in one of the major forms of nonmuscle actin, β-actin (R183W), is associated with a complicated disease phenotype that includes developmental malformations, sensory hearing loss, and a delayed-onset dystonia. To date, reports of diseases resulting from alterations of nonmuscle actins have been extremely uncommon. For β-actin, there is one report in the literature of a child with recurrent infections who exhibited a mutation at position 364 resulting from a substitution of glutamic acid to a lysine residue and causing defects in leukocyte function.[16] In contrast to the location of the mutation that we are reporting, the latter mutation was reported to reside in an actin subregion that is important for profilin binding, which facilitates nucleotide exchange within the actin monomer.[39]

In the present study, the R183W substitution replaces a flexible arginine residue with a more rigid hydrophobic tryptophan. Both database searches and testing of our own control samples failed to reveal this substitution as a polymorphism. In addition, the arginine residue at position 183 is highly conserved throughout species (fig. 2*B*). This point is further supported by observations demonstrating that mutations at the same position 183 with different amino acid substitutions, such as cysteine

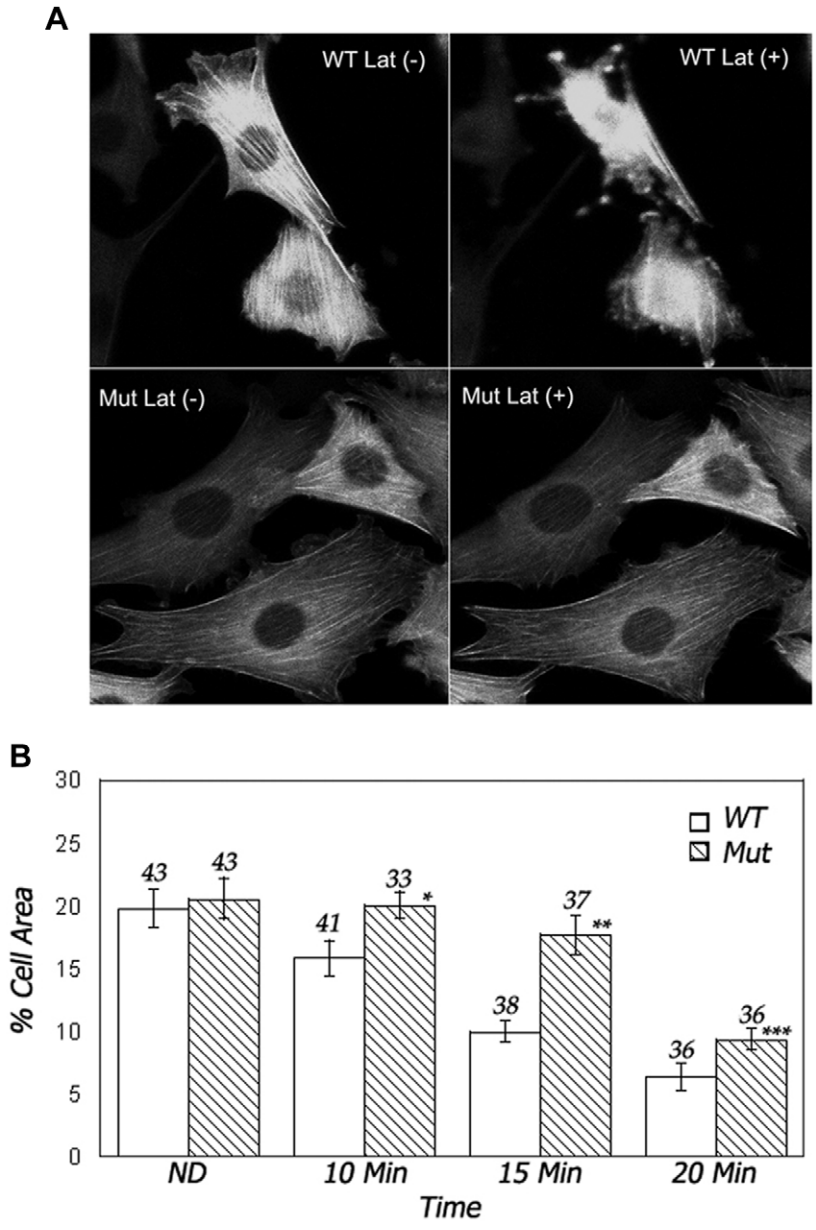

Figure 10 Latrunculin A resistance in NIH 3T3 cells expressing a GFP-tagged construct of R183W actin, compared with cells expressing a wild-type construct. *A,* Real-time confocal images of GFP-fluorescing wild-type (WT) and mutant (Mut) transfected cells before and 15 min after addition of latrunculin A (Lat) to a final concentration of 250 ng/ml. Note the loss of the stress-fiber network in the WT cells (*top left* vs. *top right panels*), in contrast to lack of significant change of stress fibers in the Mut cells (*bottom left* vs. *bottom right panels*). The images are representative of two separate experiments and a total of seven chamber cultures of WT cells and eight chamber cultures of Mut cells. The images were scanned under a 40 × oil objective. *B,* Quantitation of stress-fiber depolymerization in Mut versus WT coverslip cultures after incubation in the presence of 250 ng/ml latrunculin A for 10, 15, and 20 min. At each type point, the coverslips were rapidly rinsed and were fixed with methanol at 20°C. Confocal image series were captured from five random fields from each coverslip using a 40 × oil objective and Zeiss LSM software. LSM series were converted to TIFF files, and individual cells were analyzed for the percentage of cell area containing fluorescence with the use of Metamorph software. Image analysis for each series was performed on optical sections containing optimal visualization of the stress-fiber network. The results are from a single experiment performed using duplicate coverslips (a total of 10 fields) for each time point. ND indicates control coverslips without drug treatment. The numbers above the columns represent the cell number analyzed. P_t are .02 at 10 min, <.0001 at 15 min, and .04 at 20 min.

or glycine, have been documented in *ACTA1,* all of which result in severe myopathies.[11] These mutations exert a dominant-negative effect, which supports the concept of a "poison" protein rather than a decrease of normal actin function.[40] More than 60 mutations of *ACTA1* have been identified to date and are associated with three categories of muscle disease: (1) actin myopathy, (2) nemaline myopathy, and (3) intranuclear rod myopathy.[11,13,40,41] The characterization of these mutations in *ACTA1,* coupled with structural and functional studies of α-actin, has provided insights into genotypic-phenotypic distinctions and correlations between these different hereditary myopathies.[42]

The results of the present studies indicate that the R183W substitution affects actin dynamics in the patient lymphoblast cells and in a cell line expressing the mutant actin, and they suggest potential mechanisms by which the mutant actin form may alter the actin cytoskeletal architecture and function. First, the mutation may affect the integrity and function of the ATP-binding pocket or regions close to the pocket that are known to bind latrunculin A. Alternatively, the R183W substitution may confer greater rigidity to the filamentous molecule with lowered depolymerization dynamics. This hypothesis would explain the presence of cofilin-decorated actin inclusions in the brains of both patients.[20] Cofilin facilitates depolymerization by binding preferentially to adenosine diphosphate–rich actin filaments.[43] In vivo, the generation of small actin oligomers increases actin nucleation.[44] If the mutant filaments are resistant to normal physiologic depolymerization signals or to drugs that lower the effective concentration of ATP monomer, as with latrunculin A, then the accumulation of filamentous inclusions would be expected. Since depolymerization is the rate-limiting step in actin turnover and is critical for many biological functions, it is reasonable to hypothesize that the cellular abnormalities arising from the present mutation are linked to this defect.

The prevalence of MZ twins affected with nemaline myopathy has been reported to be higher than expected, and it has been suggested that the presence of *ACTA1* mutations might alter actin dynamics during early phases of embryogenesis.[45] In addition, our patients' phenotypes shared some clinical similarities with OS defined by midline abnormalities such as cleft lip and palate, hypertelorism, and esophageal motility abnormalities. Mutations in *MID1,* a member of the B-box protein family encoding the protein midin, have been identified in the X-linked form of OS, and these mutations have been proposed to result in altered microtubule dynamics.[46] Interestingly, MZ twinning is unusually frequent in these families and may be a consequence of analogous developmental errors.[45] Segregation analysis of microsatellite markers flanking the *ACTB* gene on chromosome 7 of our cohort demonstrates the inheritance of the same maternal alleles in the probands, which differs from one of the half-brothers (fig. 3*B*). On the basis of studies of *ACTA1* mutations, a large number of cases are sporadic, arising as de novo dominant missense mutations.[11] A small number are either compound heterozygous or recessive, and two families have been shown to have somatic mosaicism for the mutation in one of the parents.[42] Unfortunately, we were not able to examine the father of our probands to rule out this possibility.

In summary, we have identified a mutation in β-actin that is associated with several disease phenotypes, including a syndrome of ventral midline defects resembling OS,[47] sensory hearing loss, and delayed-onset generalized dystonia. The implications of these findings suggest that genetic variants of nonmuscle actins may play a wider role in human disease, analogous to the spectrum of myopathic diseases that have been associated with mutations in the muscle actin isoforms.[41] In addition, actin effects are probably mutation specific and reflect the presence of different functional domains of the monomer and filament. In fact, although numerous developmental malformation syndromes and hereditodegenerative diseases related to dystonia have been mapped to specific chromosomal loci and genes, the vast majority of these entities remain poorly understood.[17,48] Given the important actions of β-actin in all cells, it is not surprising to connect abnormalities of actin dynamics with developmental as well as neurological disorders. In fact, proteins that are known to function in concert with actin have been implicated in hereditary disorders and malformation syndromes, such as dynamin in Charcot-Marie-Tooth disease,[49] filamin in otopalatodigital syndromes,[50] as well as other conditions.[5] With respect to neural-tube closure defects, it has recently been suggested that actin abnormalities should be considered as important candidates for uncovering new pathogenic mechanisms.[51] Ongoing studies are aimed at analyzing the functional consequences of the β-actin mutation we have identified, as well as others, which should help us to understand the complex clinical phenotype of our patients.

Acknowledgments

This work was supported in part by the Alice and Roy Richards Endowed Chair (to B.H.W.); by National Institutes of Health (NIH) grants R01 AG18883 and P30 AG12300 (to E.S.), RO1 NS21328, NS41850, and AG24373 (to V.P.), RO1 NS42599 (to V.F.), and RO1 AR048615 (to S.O.); by the Foundation Jerome Lejeune (to G.M.); P30 AG10130 (M. Gearing); and by National Institute of Arthritis and Musculoskeletal and Skin Diseases Research Training Grant in Dermatology 2T32AR007587-11 (to M.S.). The authors would like to acknowledge the excellent technical assistance provided by Dr.

Viyada Nunbhakdi-Craig (University of Texas Southwestern Medical Center) and the support and insightful advice of Dr. Douglas Wallace (University of California, Irvine).

Web Resources

Accession numbers and URLs for data presented herein are as follows:

dbSNP, http://www.ncbi.nlm.nih.gov/entrez/query.fcgi?db=snp
Expasy Proteomics Server, http://us.expasy.org/tools
GenBank, http://www.ncbi.nih.gov/Genbank/ (for *ACTB* [accession number M10277], *ACTB* cDNA [accession number NM_001101], *ACTG1* cDNA [accession number NM_001614], *CFL1* cDNA [accession number NM_005507], and *ADF* cDNA [accession number NM_006870])
Marshfield Clinic, http://research.marshfieldclinic.org/genetics/Map_Markers/data/maps/Map7.txt
Online Mendelian Inheritance in Man (OMIM), http://www.ncbi.nlm.nih.gov/Omim/ (for OS)

References

1. Pollard TD, Blanchoin L, Mullins RD (2000) Molecular mechanisms controlling actin filament dynamics in nonmuscle cells. Annu Rev Biophys Biomol Struct 29:545–576
2. Chen H, Bernstein BW, Bamburg JR (2000) Regulating actin-filament dynamics in vivo. Trends Biochem Sci 25:19–23
3. Engqvist-Goldstein AE, Drubin DG (2003) Actin assembly and endocytosis: from yeast to mammals. Annu Rev Cell Dev Biol 19: 287–332
4. Yarar D, Waterman-Storer CM, Schmid SL (2005) A dynamic actin cytoskeleton functions at multiple stages of clathrin-mediated endocytosis. Mol Biol Cell 16:964–975
5. Lambrechts A, Van Troys M, Ampe C (2004) The actin cytoskeleton in normal and pathological cell motility. Int J Biochem Cell Biol 36:1890–1909
6. Garrels JI, Gibson W (1976) Identification and characterization of multiple forms of actin. Cell 9:793–805
7. Vandekerckhove J, Weber K (1978) At least six different actins are expressed in a higher mammal: an analysis based on the amino acid sequence of the amino-terminal tryptic peptide. J Mol Biol 126:783–802
8. Bamburg JR, Wiggan OP (2002) ADF/cofilin and actin dynamics in disease. Trends Cell Biol 12:598–605
9. Fechheimer M, Furukawa R, Maselli A, Davis RC (2002) Hirano bodies in health and disease. Trends Mol Med 8: 590–591
10. Gourlay CW, Ayscough KR (2005) The actin cytoskeleton: a key regulator of apoptosis and ageing? Nat Rev Mol Cell Biol 6:583–589
11. Costa CF, Rommelaere H, Waterschoot D, Sethi KK, Nowak KJ, Laing NG, Ampe C, et al (2004) Myopathy mutations in alpha-skeletal-muscle actin cause a range of molecular defects. J Cell Sci 117:3367–3377
12. Marston SB, Hodgkinson JL (2001) Cardiac and skeletal myopathies: can genotype explain phenotype? J Muscle Res Cell Motil 22:1–4
13. Clarkson E, Costa CF, Machesky LM (2004) Congenital myopathies: diseases of the actin cytoskeleton. J Pathol 204:407–417
14. Zhu M, Yang T, Wei S, DeWan AT, Morell RJ, Elfenbein JL, Fisher RA, et al (2003) Mutations in the γ-actin gene (*ACTG1*) are associated with dominant progressive deafness (DFNA20/26). Am J Hum Genet 73:1082–1091
15. van Wijk E, Krieger E, Kemperman MH, De Leenheer EM, Huygen PL, Cremers CW, Cremers FP, et al (2003) A mutation in the gamma actin 1 (ACTG1) gene causes autosomal dominant hearing loss (DFNA20/26). J Med Genet 40:879–884
16. Nunoi H, Yamazaki T, Tsuchiya H, Kato S, Malech HL, Matsuda IKanegasaki S (1999) A heterozygous mutation of beta-actin associated with neutrophil dysfunction and recurrent infection. Proc Natl Acad Sci USA 96:8693–8698
17. Nemeth AH (2002) The genetics of primary dystonias and related disorders. Brain 125:695–721
18. de Carvalho Aguiar PM, Ozelius LJ (2002) Classification and genetics of dystonia. Lancet Neurol 1:316–325
19. Ozelius LJ (2004) Update on the genetics of primary torsion dystonia loci DYT6, DYT7, and DYT13 and the dystonia-plus locus DYT12. Adv Neurol 94:109–112
20. Gearing M, Juncos JL, Procaccio V, Gutekunst CA, Marino-Rodriguez EM, Gyure KA, Ono S, et al (2002) Aggregation of actin and cofilin in identical twins with juvenile-onset dystonia. Ann Neurol 52:465–476
21. Trounce IA, Kim YL, Jun AS, Wallace DC (1996) Assessment of mitochondrial oxidative phosphorylation in patient muscle biopsies, lymphoblasts, and transmitochondrial cell lines. Methods Enzymol 264:484–509
22. Robin NH, Feldman GJ, Aronson AL, Mitchell HF, Weksberg R, Leonard CO, Burton BK, et al (1995) Opitz syndrome is genetically heterogeneous, with one locus on Xp22, and a second locus on 22q11.2. Nat Genet 11:459–461
23. Quaderi NA, Schweiger S, Gaudenz K, Franco B, Rugarli EI, Berger W, Feldman GJ, et al (1997) Opitz G/BBB syndrome, a defect of midline development, is due to mutations in a new RING finger gene on Xp22. Nat Genet 17:285–291
24. Gaudenz K, Roessler E, Quaderi N, Franco B, Feldman G, Gasser DL, Wittwer B, et al (1998) Opitz G/BBB syndrome in Xp22: mutations in the MID1 gene cluster in the carboxy-terminal domain. Am J Hum Genet 63:703–710 (erratum 63:1571)
25. McDonald-McGinn DM, Emanuel BS, Zackai EH (1996) Autosomal dominant "Opitz" GBBB syndrome due to a 22q11.2 deletion. Am J Med Genet 64:525–526
26. Minamide LS, Bamburg JR (1990) A filter paper dye-binding assay for quantitative determination of protein without interference from reducing agents or detergents. Anal Biochem 190:66–70
27. Wessel D, Flugge UI (1984) A method for the quantitative recovery of protein in dilute solution in the presence of detergents and lipids. Anal Biochem 138:141–143
28. Nunbhakdi-Craig V, Craig L, Machleidt T, Sontag E (2003) Simian virus 40 small tumor antigen induces deregulation of the actin cytoskeleton and tight junctions in kidney epithelial cells. J Virol 77:2807–2818
29. Wertman KF, Drubin DG, Botstein D (1992) Systematic mutational analysis of the yeast ACT1 gene. Genetics 132:337–350
30. Ayscough KR, Stryker J, Pokala N, Sanders M, Crews P, Drubin DG (1997) High rates of actin filament turnover in budding yeast and roles for actin in establishment and maintenance of cell polarity revealed using the actin inhibitor latrunculin-A. J Cell Biol 137:399–416
31. Fujita M, Ichinose S, Kiyono T, Tsurumi TO, Mori A (2003) Establishment of latrunculin-A resistance in HeLa cells by expression of R183A D184A mutant beta-actin. Oncogene 22:627–631
32. Leavitt J, Ng SY, Aebi U, Varma M, Latter G, Burbeck S, Kedes L, et al (1987) Expression of transfected mutant beta-actin genes: alterations of cell morphology and evidence for autoregulation in actin pools. Mol Cell Biol 7:2457–2466
33. Lloyd C, Schevzov G, Gunning P (1992) Transfection of nonmuscle beta- and gamma-actin genes into myoblasts elicits different feedback regulatory responses from endogenous actin genes. J Cell Biol 117:787–797
34. Vorobiev S, Strokopytov B, Drubin DG, Frieden C, Ono S, Con-

deelis J, Rubenstein PA, et al (2003) The structure of nonvertebrate actin: implications for the ATP hydrolytic mechanism. Proc Natl Acad Sci USA 100:5760–5765
35. Wriggers W, Schulten K (1999) Investigating a back door mechanism of actin phosphate release by steered molecular dynamics. Proteins 35:262–273
36. Belmont LD, Patterson GM, Drubin DG (1999) New actin mutants allow further characterization of the nucleotide binding cleft and drug binding sites. J Cell Sci 112:1325–1336
37. Morton WM, Ayscough KR, McLaughlin PJ (2000) Latrunculin alters the actin-monomer subunit interface to prevent polymerization. Nat Cell Biol 2:376–378
38. Klein C, Liu L, Doheny D, Kock N, Muller B, de Carvalho Aguiar P, Leung J, et al (2002) Epsilon-sarcoglycan mutations found in combination with other dystonia gene mutations. Ann Neurol 52: 675–679
39. Witke W (2004) The role of profilin complexes in cell motility and other cellular processes. Trends Cell Biol 14:461–469
40. Ilkovski B, Nowak KJ, Domazetovska A, Maxwell AL, Clement S, Davies KE, Laing NG, et al (2004) Evidence for a dominant-negative effect in ACTA1 nemaline myopathy caused by abnormal folding, aggregation and altered polymerization of mutant actin isoforms. Hum Mol Genet 13:1727–1743
41. Nowak KJ, Wattanasirichaigoon D, Goebel HH, Wilce M, Pelin K, Donner K, Jacob RL, et al (1999) Mutations in the skeletal muscle alpha-actin gene in patients with actin myopathy and nemaline myopathy. Nat Genet 23:208–212
42. Wallgren-Pettersson C, Pelin K, Nowak KJ, Muntoni F, Romero NB, Goebel HH, North KN, et al (2004) Genotype-phenotype correlations in nemaline myopathy caused by mutations in the genes for nebulin and skeletal muscle alpha-actin. Neuromuscul Disord 14:461–470
43. Carlier MF, Laurent V, Santolini J, Melki R, Didry D, Xia GX, Hong Y, et al (1997) Actin depolymerizing factor (ADF/cofilin) enhances the rate of filament turnover: implication in actin-based motility. J Cell Biol 136:1307–1322
44. Ghosh M, Song X, Mouneimne G, Sidani M, Lawrence DS, Condeelis JS (2004) Cofilin promotes actin polymerization and defines the direction of cell motility. Science 304:743–746
45. Graziano C, Bertini E, Porfirio B (2005) De novo alpha-actin mutations in monozygotic twins. Clin Genet 68:91–92
46. So J, Suckow V, Kijas Z, Kalscheuer V, Moser B, Winter J, Baars M, et al (2005) Mild phenotypes in a series of patients with Opitz GBBB syndrome with MID1 mutations. Am J Med Genet A 132: 1–7
47. Robin NH, Opitz JM, Muenke M (1996) Opitz G/BBB syndrome: clinical comparisons of families linked to Xp22 and 22q, and a review of the literature. Am J Med Genet 62:305–317
48. Hobbs CA, Cleves MA, Simmons CJ (2002) Genetic epidemiology and congenital malformations: from the chromosome to the crib. Arch Pediatr Adolesc Med 156:315–320 (erratum 156:1051)
49. Zuchner S, Noureddine M, Kennerson M, Verhoeven K, Claeys K, De Jonghe P, Merory J, et al (2005) Mutations in the pleckstrin homology domain of dynamin 2 cause dominant intermediate Charcot-Marie-Tooth disease. Nat Genet 37:289–294
50. Hidalgo-Bravo A, Pompa-Mera EN, Kofman-Alfaro S, Gonzalez-Bonilla CR, Zenteno JC (2005) A novel filamin A D203Y mutation in a female patient with otopalatodigital type 1 syndrome and extremely skewed X chromosome inactivation. Am J Med Genet A 136:190–193
51. Juriloff DM, Harris MJ (2000) Mouse models for neural tube closure defects. Hum Mol Genet 9:993–1000